Int. J. Environ. Sci. Technol. (2015) 12:3095–3106
DOI 10.1007/s13762-014-0682-0

ORIGINAL PAPER

Kinetic and isotherm analysis for selective thorium(IV) retrieval from aqueous environment using eco-friendly cellulose composite

P. D. Bhalara · D. Punetha · K. Balasubramanian

Received: 17 January 2014 / Revised: 12 August 2014 / Accepted: 7 October 2014 / Published online: 19 October 2014
© Islamic Azad University (IAU) 2014

Abstract Thorium reclamation was studied using nano-iron oxide-impregnated cellulose acetate beads to gain insights into the adsorption mechanism, kinetics and thermodynamics. The designed experiments were thoroughly investigated as a function of solution pH, initial thorium(IV) ion concentration, adsorbent dose and nano-iron oxide loading in the cellulose acetate matrix. The batch adsorption of Th(IV) ions revealed the highly pH dependent (pH range 3.0–9.0) behaviour with maximum sorption at pH 6.0 and equilibrium being achieved within 2 h for maximum concentration of 100 mg/L at 298 K. Rapid adsorption of 50 ± 0.2 % was observed within first 10 min. The kinetics data are best described by the pseudo-first-order kinetic model ($R^2 = 0.9996$) and intraparticle diffusion model. The equilibrium adsorption process was fitted with the Langmuir, Freundlich, Dubinin–Radushkevich and Temkin models which yield good fit with Langmuir isotherm equation indicating monolayer adsorption process. The calculated thermodynamics parameter reveals spontaneous and exothermic adsorption process. Further, the desorption was Th(IV) ions that was easily achieved using 0.05 N HNO_3 which suggests the reusability of the adsorbent for multiple use.

Keywords Thorium(IV) · Cellulose · Adsorption · Diffusion · Kinetics and isotherms

Introduction

Environmental disquiets associated with the disposal of radioactive toxic metal ions such as thorium(IV) in water bodies and effluents have stimulated the development of enhanced materials proficient in eliminating the contaminants from direct surroundings (Anirudhan et al. 2010; Kütahyalı and Eral 2010; Shtangeeva et al. 2005; Kaygun and Akyil 2007; Anirudhan and Jalajamony 2013; Nilchi et al. 2013; Akkaya and Akkaya 2013; Baybaş and Ulusoy 2012; Seyhan et al. 2008; Anirudhan et al. 2013b). Severe environmental concerns force the establishment for progressively more stringent governmental norms, demanding lower levels of contaminant (Marmolejo-Rodríguez et al. 2008; Sunta et al. 1987). Thorium(IV) is extensively used for various applications in optics, radio, aeronautics and aerospace, metallurgy and chemical industry, nuclear industry and material field (Zhang et al. 2005). It forms an important constituent of the fuel in nuclear breeder reactors, and thorium fuel cycle can be used in most of the reactors already operated (Raje and Reddy 2010; Ünak 2000). The health hazards associated with this radionuclide arise from its ability to accumulate in human tissues. Thorium nitrate after entering into living organisms localizes mainly in the liver, spleen and marrow and precipitates in the form of hydroxide causing harmful diseases in human beings, such as lung, pancreatic and liver cancer

P. D. Bhalara
Department of Ceramic Engineering, Indian Institute of Technology (BHU), Varanasi 221005, India

D. Punetha
School of Material Science and Technology, Indian Institute of Technology (BHU), Varanasi 221005, India

K. Balasubramanian (✉)
Department of Materials Engineering, Defence Institute of Advanced Technology (DU), Ministry of Defence, Girinagar, Pune 411025, India
e-mail: meetkbs@gmail.com

(Valković 2000). The maximum permissible limit for thorium in drinking water is 150 μg/L (DeZuane 1997).

Solvent extraction (Borowiak-Resterna et al. 2010), chemical precipitation (Soylak and Erdogan 2006; Uluozlu et al. 2010), reverse osmosis and membrane separation (Kosarek 1979; Prabhakar et al. 1994), ion exchange (Shoushtari et al. 2006), electro-floatation (Aydin and Soylak 2010), coagulation (El Samrani et al. 2008) and sorption processes (Rule et al. 2014) are some of the indigenous techniques for removing heavy metal ions from aqueous solution. The separation of small amounts of substances from large volume of solution can be efficiently and conveniently carried out using adsorption. Adsorption is the technique preferably used due to its ease of operation, flexibility and simplicity of design, and the separation of small amounts of substances from large volume of solution can be efficiently and conveniently carried out. The challenges associated with adsorption include increase in sorption capacity, separability and cost-effectiveness (Babel and Kurniawan 2003). Various materials have been investigated as adsorbents for thorium adsorption (Table 1), such as activated carbons (Metaxas et al. 2003), gibbsite (Hongxia et al. 2006), silica (Chen and Wang 2007), bentonite (Zhao et al. 2008), *Pseudomonas* sp. (Kazy et al. 2009), *Aspergillus fumigatus* (Bhainsa and D'Souza 2009) and perlite (Talip et al. 2009).

Also, some nanomaterials have been focused on as adsorbents for heavy metal ions in water and proven to be promising for environmental remediation (Zhao et al. 2013). Owing to the unique physical and chemical properties such as large specific surface areas, high adsorption capacity and fast adsorption rate, nanomaterials have shown remarkable potential to capture toxic pollutants from water. On the other hand, due to their easy suspension in water, it is quite difficult to remove these nanomaterials from large volumes of water, which limits their practical application (Pereira et al. 2013; Klaine et al. 2008; Cao et al. 2010; Yuan 2004; Zhang and Fang 2010). An effective strategy to solve this problem is to embed these nanomaterials in insoluble cellulose composite to synthesis an efficient adsorbent.

In the present work, nano-iron oxide (Fe_2O_3)-impregnated cellulose acetate composites beads with varying nano-iron oxide (Fe_2O_3) content were synthesized by precipitation polymerization technique for the removal and recovery of Th(IV) ions from mimicked contaminated water. Surface morphology of the adsorbent was studied using scanning electron microscopy (JOEL ASM 6360A). Adsorption of Th(IV) was studied as a function of solution pH, initial Th(IV) ion concentration, adsorbent dose, additive (nano-iron oxide) concentration and contact time at ambient temperature. Adsorption was spectrophotometerically monitored periodically to study the equilibrium isotherms and kinetic mechanism using various mathematical models. Desorption of Th(IV) was also experimented to determine the reusability of the present adsorbent system. Thus, the main aim of this study was to synthesis a highly effective eco-friendly adsorbent which is economical that helps us to combat the contamination generated by hazardous Th(IV) ions.

Table 1 Adsorption of thorium(IV) ions by various adsorbents

Adsorbent	pH	q_e (μmol/g)	References
Gibbsite	4	4	Hongxia et al. (2006)
Silica	3.5	1	Chen and Wang (2007)
Silica + humic acid	3.5	2.05	
Silica + Fulvic acid	3.5	2.45	
Bentonite	4	2.75	Zhao et al. (2008)
Perlite	4.5	5	Talip et al. (2009)

Materials and methods

Materials

Thorium nitrate, cellulose acetate, nano-iron oxide (Fe_2O_3), arsenazo(III), dimethyl acetamide and acetone (99.8 %) were obtained from Sigma-Aldrich, India, and were used as received. Deionized water was used in the present study. Stock solution of 100 mg/L of thorium(IV) ions was prepared, and the desired concentrations were obtained by diluting this stock solution.

Synthesis of iron oxide-impregnated cellulose acetate beads

The nano-iron oxide (Fe_2O_3)-impregnated cellulose acetate beads used for the adsorption process were synthesized (Ayalew et al. 2012; Gonte et al. 2013a) by dissolving the requisite amount of cellulose acetate, NaCl and NaOH in 1:2 ratio of DMA/acetone solution to obtain a homogenous mixture. Five different compositions were prepared by varying the nano-iron oxide (Fe_2O_3) content from 2 to 8 wt%. This mixture was precipitated in dilute HCl bath (coagulation) to obtain the uniform-sized spherical polymer beads. These beads were purified by continuous water washing for 2–3 times and finally air-dried to constant weight.

Characterization

The surface morphology of the adsorbent was observed using scanning electron microscope (JOEL ASM 6360A). The concentration of the residual Th(IV) ions was spectrophotometerically evaluated at 665 nm using Systronics 166 UV–Visible Spectrophotometer by complexing with arsenazo(III).

Batch adsorption experiments

Adsorption of Th(IV) was analysed by agitating 50 mL solution containing 25, 50, 75 and 100 mg/L of Th(IV) ion concentration with 0.2 g beads for 120 min. The solution was periodically monitored to detect the concentration of the metal ions remaining in the solution. The effect of solution pH on adsorption was observed by changing the solution pH from pH 3 to pH 9 for a fixed concentration and volume. The pH of the solution was adjusted using dilute acetic acid and dilute ammonium hydroxide. The amount of beads was also varied from 0.05 to 0.4 g to obtain another set of data.

Equilibrium isotherms

Adsorption isotherms are plots of equilibrium adsorption capacity (q_e) versus equilibrium concentration of the residual metal ions in the solution (C_e). Adsorption isotherm studies were conducted at constant temperature 298 K and under optimized conditions. Absorbance was regularly noted after fixed time interval of 15 min. The equilibrium adsorption capacity was calculated using

$$q_e = (C_0 - C_e)V/M \quad (1)$$

where q_e (mg/g) is the equilibrium adsorption capacity, C_0 and C_e are initial and equilibrium concentration (mg/L) of metal ions in solution, V (L) is volume of solution and M (g) is the weight of the adsorbent.

Kinetic studies

Kinetic experiments were conducted using known weight of cellulose acetate beads and varying initial metal ion concentration. The samples were tested at regular time intervals (0–120 min) for concentration of metal ions. The rate constants were calculated using the conventional rate expression. The amount of metal ion sorbed, q_t, was calculated as follows:

$$q_t = (C_0 - C_e)V/M \quad (2)$$

where q_t (mg/g) is the adsorption capacity at time t.

Results and discussion

Synthesis and characterization of nano-iron oxide (Fe_2O_3)-impregnated cellulose acetate beads

Uniform-sized spherical beads with the homogeneous distribution of nano-iron oxide (Fe_2O_3) were obtained by precipitation polymerization technique as shown in Fig. 1a. Beads with varying nano-iron oxide (Fe2O3) content were obtained by sonicating (Sonicator Model. EI-6LH-SP, Sl. No. 1209-122, India) 2–8 wt% nano-iron oxide (Fe2O3) in the mixture at 20 kHz and 20 W. The obtained bead possessed an average diameter of 0.5 mm without any tailing effect. The nozzle diameter and the height between the dilute HCl bath (coagulation) and the nozzle were found to play a key role in controlling the bead diameter and tailing effect which were optimized to 0.1 mm and 5 cm, respectively. Optical images of the beads demonstrated hexagonal-shaped beehive-like pores present on the surface (Fig. 1b). The SEM micrographs (Fig. 1c, d) further revealed the presence of well-defined flow lines indicating capillary action introduced in the polymer matrix. The presence of OH^- ions tends to replace the acetate ions from cellulose acetate and increase its activity (Hornback 2005). Oozing of NaCl and NaOH from the polymer mixture which ex-filtrates out from the beads is found to be responsible for the introduction of capillary action which enhances the adsorption capacity.

Effect of various experimental parameters

Solution pH

The pH of the aqueous solution plays an important role and influences the metal speciation and surface metal-binding sites (Clark et al. 2011). Adsorption was studied by varying the pH from 3 to 9 for fixed Th(IV) conc. Adsorption of Th(IV) increased with an increase in pH from pH 3 to 6 (Fig. 2a).

Th(IV) ions tend to precipitate in form of hydroxide with further increase in pH. Decrease in adsorption at lower pH can be explained by the protonation of the adsorbent molecules, which causes repulsion of the positively charged thorium ions and steric hindrance by the protonated ions. Figure 3 shows the distribution of thorium species versus pH at 298 K in aqueous solution (Langmuir and Herman 1980). Free Th(IV) ion dominates at pH's below 3.

At pH value 6, $Th(OH)^{3+}$, $Th(OH)_2^{2+}$, $Th_2(OH)_2^{6+}$ and $Th_6(OH)_{15}^{9+}$ appear as the predominant ionic species (Langmuir and Herman 1980) and the solubility of thorium decreases significantly. Hence, all the adsorption experiments were carried out at pH 6. The following mechanism for metal ions removal was expected:

$$1/2\left[M(H_2O)_6\right]^{n+} + OH^- \leftrightarrow \left[M(OH)(H_2O)_5\right]^{(n-1)} + H_2O \quad (a)$$

$$\left[M(OH)(H_2O)_5\right]^{(n-1)+} + OH^- \leftrightarrow \left[M(OH)_2(H_2O)_4\right]^{(n-2)+} + H_2O \quad (b)$$

$$\left[M(OH)_2(H_2O)_6\right] \leftrightarrow M(OH)_2\downarrow + 4H_2O \quad (c)$$

Baes et al. (1965) suggest the corner-sharing bidentate-mononuclear surface complex, $(>FeO)_2Th^{2+}$, being responsible for Th(IV) binding on the iron oxide surface.

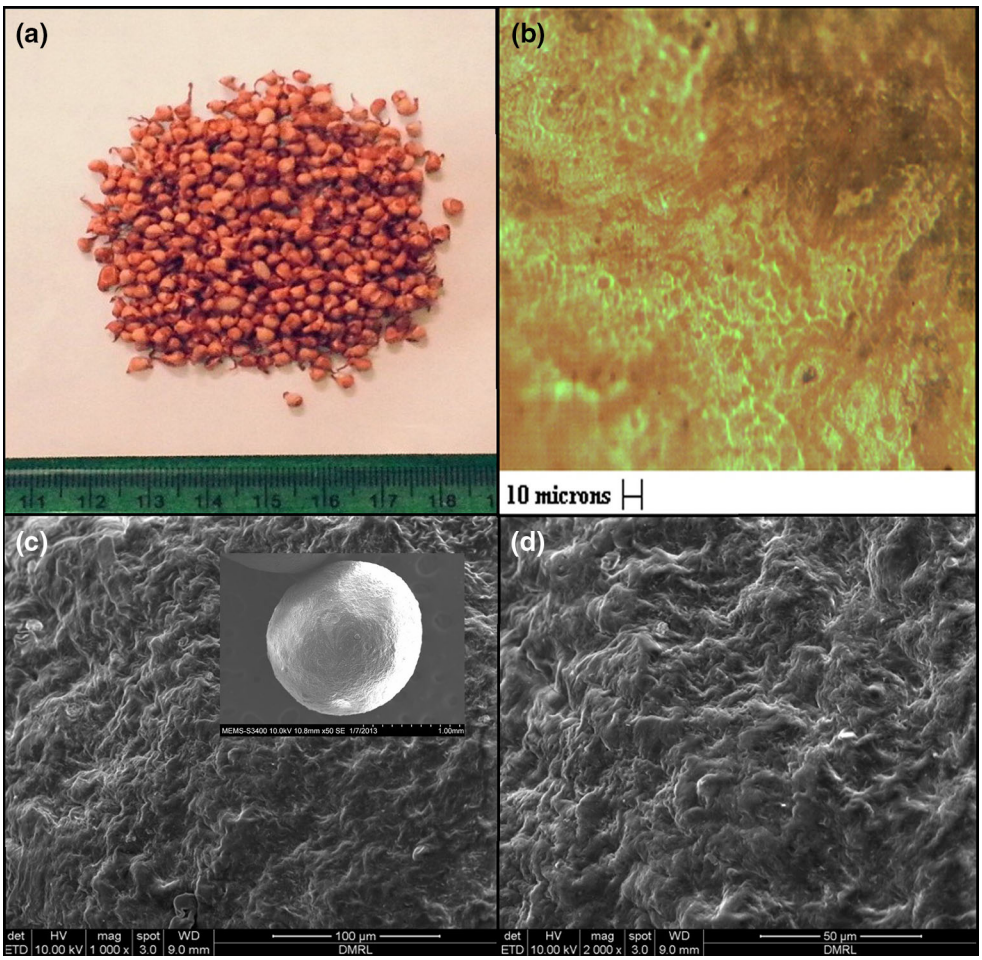

Fig. 1 Nano-iron oxide (Fe_2O_3)-impregnated cellulose beads: **a** digital image, **b** optical image, **c** SEM micrograph (*inset* low-magnification SEM), **d** SEM magnified surface view

Nano-iron oxide (Fe_2O_3) content in the beads

Beads with varying amount of nano-iron oxide (Fe_2O_3) were synthesized, and their adsorption capacity was evaluated. Adsorption was found to increase with increase in nano-iron oxide (Fe_2O_3) content from 2 to 4 wt% (Fig. 2b). Further increase in the iron oxide content resulted in decrease in adsorption. The initial increase is attributed to increase in adsorption sites due to increased surface area with the addition of sorbent particles. The decrease in adsorption beyond 4 wt% is attributed to decreased porosity of the beads due to the excess amount of additive. Steric affect also plays a role in lowering of adsorption.

Effect of sorbent dose on thorium adsorption

It was observed that adsorption increases with increase in adsorbate dose from 0.05 to 0.3 g (Fig. 2c). Removal of metal ions increases with increased adsorbent dosage due to increase in active sites. As the Th(IV) ions are distributed throughout the liquid medium, which makes it difficult to trap, relatively more amount of adsorbent quantity is consumed. The equilibrium attained in the later stages may be due to a larger number of active sites as compared to the number of thorium ions. Hence, for a greater amount of adsorbent, adsorption remains unaffected with increase in the adsorbent dose.

Effect of initial metal concentration

The adsorption efficiency was found to decreases with increase in the initial metal ion concentration, whereas increase in the initial metal ion concentration results in increased adsorption capacity (Fig. 2d) since the high-concentration gradient provides a driving force to overcome all mass transfer resistances of metal ions between the aqueous and solid phase. The sorption efficiency decreases due to the limited number of active sites of the adsorbent, which saturates at a certain concentration. This

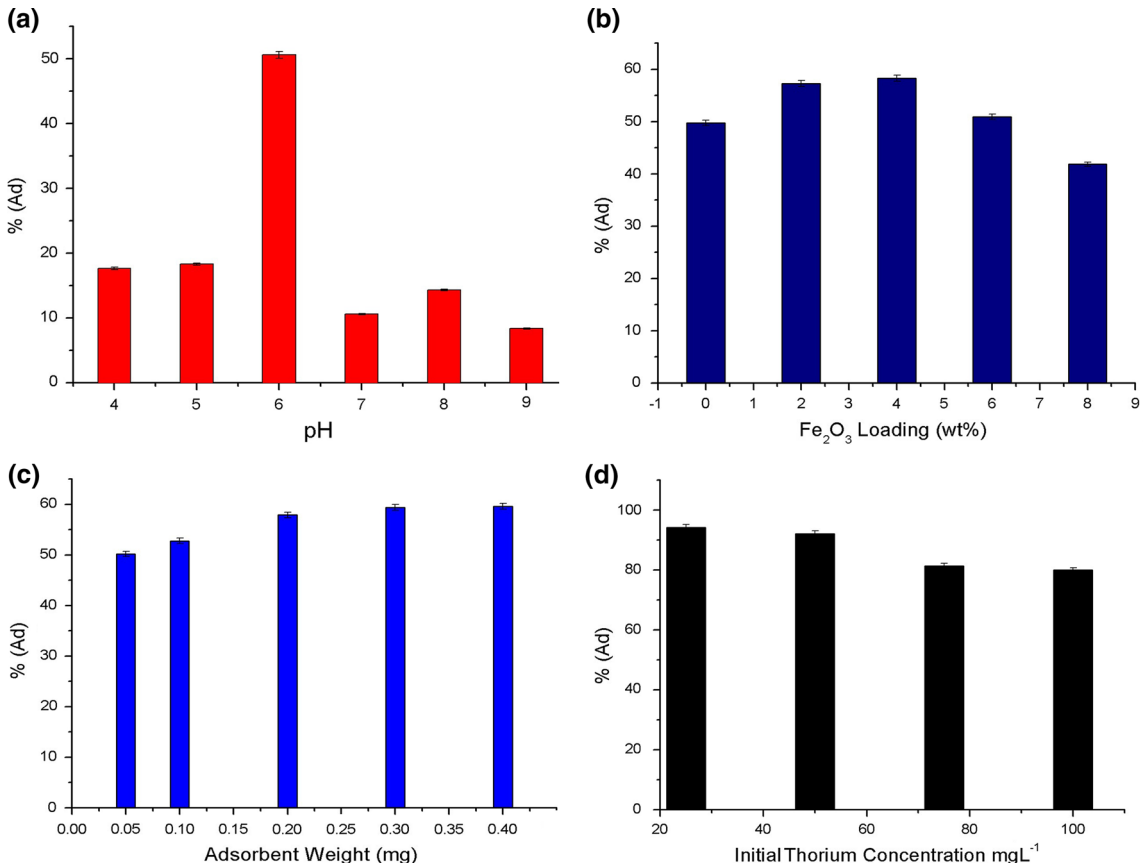

Fig. 2 Effect of **a** pH on adsorption, **b** nano-iron oxide (Fe2O3) loading on adsorption, **c** adsorbent dose on adsorption, **d** initial thorium(IV) conc on adsorption

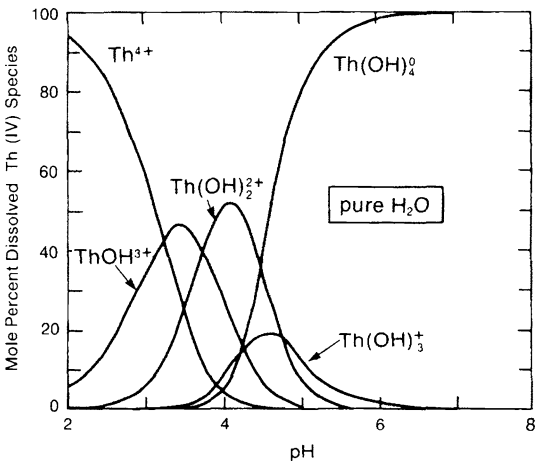

Fig. 3 Distribution of thorium-hydroxy complexes versus pH at 298 K (Langmuir and Herman 1980)

indicates that though the adsorption capacity will increase with the increase in initial concentration, the concentration will inversely impact the adsorption efficiency because of the limited adsorption sites available for the uptake of metal ions.

Isotherm studies

Adsorption isotherm studies are important to determine the efficiency of adsorption. The adsorption isotherm indicates how the adsorption molecules distribute between the liquid phase and the solid phase when the adsorption process reaches an equilibrium state. The adsorption mechanism and adsorbent's affinity for the metal ion can be determined by analysing the physicochemical parameters (Bulut et al. 2008; Febrianto et al. 2009; Gonte et al. 2013b; Gonte and Balasubramanian 2013). There are several isotherm equations available for analysing experimental adsorption equilibrium data. Several adsorption isotherms originally used for gas-phase adsorption are available and readily adopted to correlate adsorption equilibria in heavy metals adsorption. Some well-known ones are Freundlich, Langmuir, Temkin, Redlich–Paterson and Sips equations (Febrianto et al. 2009; Gonte et al. 2013b; Gonte and Balasubramanian 2013). In this study, the experimental equilibrium data for adsorbed metal ions onto nano-iron oxide (Fe_2O_3)-impregnated cellulose acetate beads were analysed using the Langmuir, Freundlich, Temkin and D–R models. The isotherm constants for the four models were obtained by linear regression methods. These isotherms are as follows:

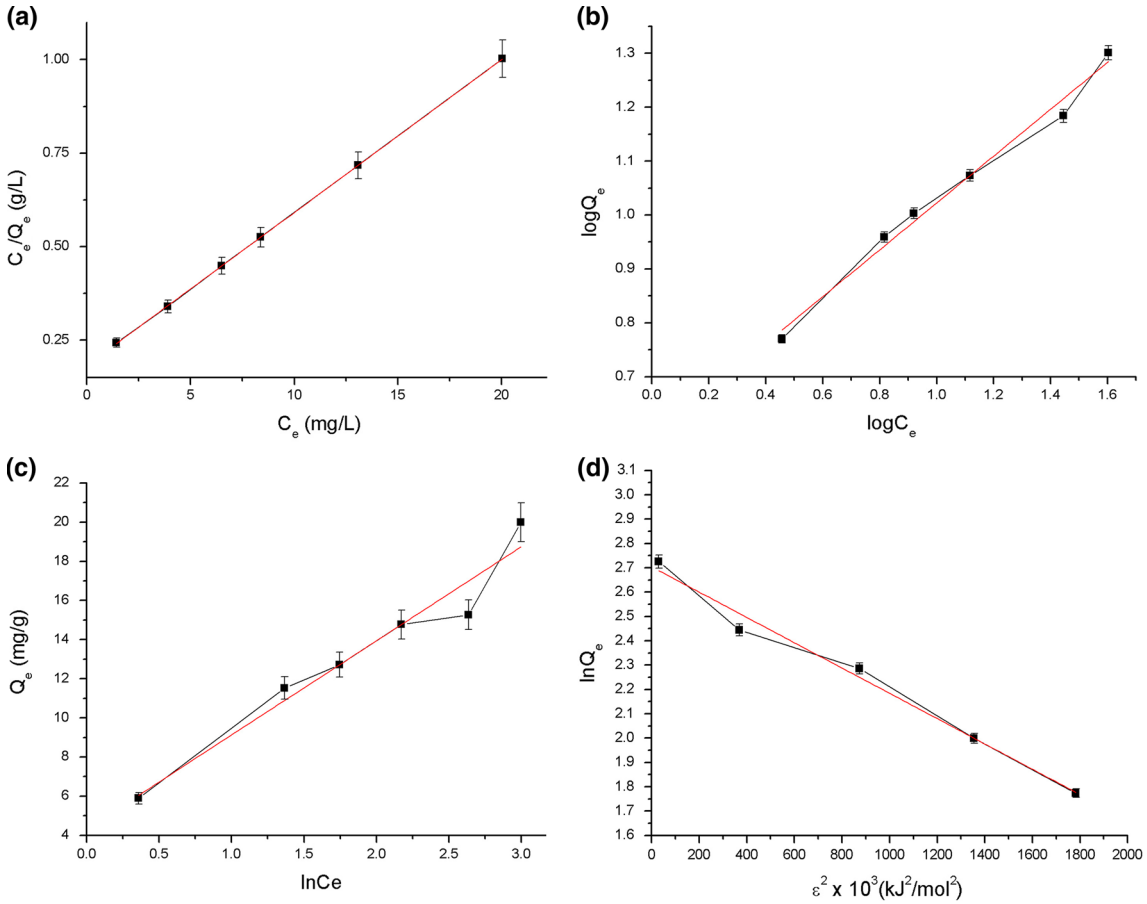

Fig. 4 Equilibrium adsorption models. **a** Langmuir, **b** Freundlich, **c** Temkin, **d** D–R

Langmuir isotherm model

The Langmuir model assumes that a monomolecular layer is formed when adsorption takes place without any interaction between the adsorbed molecules (Aksu 2002). The Langmuir model can be represented as follows:

$$q_e = \frac{q_{max} K_L C_e}{1 + K_L C_e} \tag{3}$$

where q_{max} is q_e for a complete monolayer (mg/g) and K_L is a constant related to the affinity of the binding sites (L/mg). The linearized form of the Langmuir equation is as follows:

$$\frac{C_e}{q_e} = \frac{1}{q_{max} K_L} + \frac{C_e}{q_{max}} \tag{4}$$

The experimental data were plotted as C_e/q_e versus C_e (Fig. 4a), and the values of Langmuir constants q_{max} and b were obtained by linear regression method which exhibited high correlation with Langmuir model within the studied temperature range. The essential features of a Langmuir isotherm can be expressed in terms of a dimensionless constant separation factor or equilibrium parameter, R_L which is defined (Hall et al. 1966) as follows:

$$R_L = \frac{1}{1 + K_L C_0} \tag{5}$$

where K_L (L/mg) is the Langmuir constant and C_0 (mg/L) is the initial concentration. The value of R_L provides information as to whether the adsorption is irreversible ($R_L = 0$), favourable ($0 < R_L < 1$), linearly favourable ($R_L = 1$) or unfavourable ($R_L > 1$). The value of R^2 calculated from Langmuir model was 0.9996 suggesting this to be the appropriate isotherm for the adsorption. The value of q_{max} using this model was found to be 24.43 mg/g. R_L value of 0.15 indicates that the reaction is favourable.

Freundlich isotherm model

The Freundlich isotherm model gives an empirical expression expressing the isothermal variation of the adsorbed quantity of metal ion by unit mass of solid adsorbent with concentration, taking into account

heterogeneous adsorption surfaces. The adsorption capacity is correlated with the concentration of metal ions at equilibrium. The Freundlich adsorption isotherm is mathematically expressed as follows:

$$q_e = (K_F C_e)^{1/n} \quad (6)$$

where K_F and n are Freundlich constants for a given adsorbate and adsorbent pair. The linearized form of Freundlich equation is given as follows:

$$\log q_e = \frac{1}{n}\log C_e + \log K_F \quad (7)$$

The maximum sorption capacity can be determined by varying the sorbent dose while keeping the initial concentration constant. The extrapolated value of log x/m for $C_e = C_0$ gives the maximum adsorption capacity (Gonte and Balasubramanian 2013; Aksu 2002; Hall et al. 1966). The value of n and K_F can be determined by plotting a graph between log q_e and log C_e and analysing the slope and intercept of the curve (Fig. 4b). Freundlich constant n value between one and ten indicates favourable adsorption. The value of n and K_L from the curve was calculated to be 2.30 g/L and 3.87 mg/g. R^2 value was found to be 0.9887 for Freundlich isotherm model.

Temkin isotherm model

Temkin isotherm considers the effects of the heat of adsorption that decreases linearly with coverage of the adsorbate and adsorbent interactions (Choy et al. 1999). The Temkin isotherm has been used in the form as follows:

$$q_e = \frac{RT}{b_T} \times \ln(a_T C_e) + \frac{RT}{b_T}\ln C_e \quad (8)$$

where R is gas constant 8.314×10^{-3} kJ/mol/K; T is absolute temperature (Kelvin); b_T is the Temkin constant related to the heat of adsorption (kJ/mol) and a_T is the equilibrium binding constant corresponding to the maximum binding energy (L/g). The liner plots of q_e versus log C_e (Fig. 4c) enable to determine the constants a_T and b_T which were calculated to be 0.89 and 0.522, respectively. R^2 value of 0.9462 makes this model unfavourable for this adsorption process.

Dubinin–Radushkevich isotherm model

Dubinin (Rengaraj et al. 2004) proposed the isotherm to estimate the mean free energy of adsorption. The Dubinin–Radushkevitch (D–R) isotherm describes the adsorption on a single type of uniform pores and is applied to distinguish between physical and chemical adsorption. This isotherm does not assume a homogeneous surface or a constant adsorption potential. The nonlinear D–R isotherm is expressed as follows:

$$q_e = q_{max} e^{\left(-K_D \varepsilon^2\right)} \quad (9)$$

where K (mol^{2}k/J^2) is a constant related to the mean adsorption energy and ε is the Polanyi potential, which can be calculated from equation

$$\varepsilon = RT \ln\left(1 + \frac{1}{C_e}\right) \quad (10)$$

The linear form of the equation is as follows:

$$\ln q_e = \ln q_{max} - K\varepsilon^2 \quad (11)$$

The plot between ln q_e and ε^2 at fixed temperature yields the constant K and q_{max} (Fig. 4d). The value of K was calculated to be 5.2×10^{-7}, and q_{max} was found to be 14.93. The constant K provides the mean free energy sorption per molecule of the sorbate when it is transferred to the surface of the solid from infinity in the solution, represented as E, and can be computed using (Rengaraj et al. 2004)

$$E = \frac{1}{\sqrt{2K}} \quad (12)$$

As per the D–R model, this value was 13.6×10^5 kJ.

The equilibrium isotherm curves and parameters for the various models are summarized in Fig. 4 and Table 2, respectively.

Table 2 Equilibrium isotherm parameters

Adsorption isotherm models	Isotherm parameters	
Langmuir	q_{max}	24.43
	R_L	0.15
	R^2	0.9996
	K_L	0.2154
Freundlich	K_F	3.87
	n	2.30
	R^2	0.9887
Temkin	a_T	0.89
	b_T	0.52
	R^2	0.9462
Dubinin–Radushkevich	q_{max}	14.93
	K_D	5.2×10^{-7}
	E	13.6×10^5
	R^2	0.9787

Kinetic studies

Kinetic models have been exploited to analyse the experimental data and investigate the mechanism of adsorption

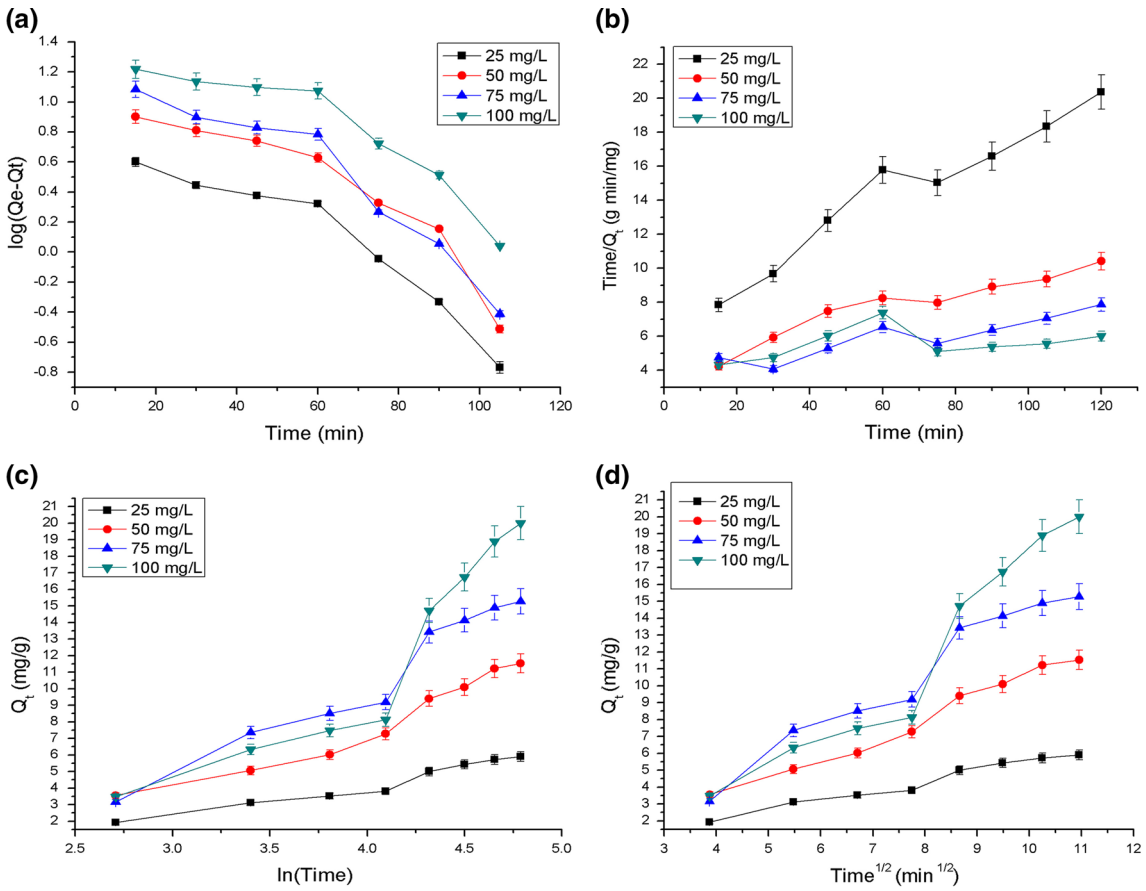

Fig. 5 Adsorption kinetic models. **a** Pseudo-first order, **b** pseudo-second order, **c** Elovich, **d** intra-particle diffusion

and its potential rate-controlling steps that include mass transport and chemical reaction processes. In addition, information on the kinetics of metal uptake is required to select the optimum condition for full-scale batch metal removal processes. The prediction of the rate-limiting step is an important factor to be considered in the adsorption process (Sarkar et al. 2003).

Pseudo-first-order kinetic model

To avoid complication and cost of a second-order reaction, it is treated as a pseudo-first order, wherein the concentration of one component is taken significantly higher than the other one.

$$R = k[A][B] \tag{13}$$

Since the concentration of one of the components, say A, is very high in comparison with that of B, we can assume $[A]$ to be constant. Hence, the equation reduces to

$$R = k'[B] \tag{14}$$

where k' is $k[A]$.The rate of adsorption of solute on the adsorbent is based on the adsorption capacity and follows pseudo-first-order equation which is often used to estimate the k_{ad}, mass transfer coefficient in the design calculations (Anirudhan et al. 2013a; Frost and Pearson 1961). The pseudo-first-order rate equation is given as follows:

$$\log(q_e - q_t) = \log q_e - \left(\frac{k_1}{2.303}\right)t \tag{15}$$

k_1 is the first-order adsorption rate constant (min^{-1}).

The plot of log (q_e–q_t) versus t yields a straight line with negative slope as shown in Fig. 5a. The intercept yields the value of q_e, whereas the pseudo-first-order constant is derived from the slope of the straight line.

Pseudo-second-order kinetic model

The pseudo-second-order reaction is greatly influenced by the amount of metal on the adsorbent's surface and the amount of metal adsorbed at equilibrium. The rate is directly proportional to the number of active surface sites (Gonte et al. 2013b). The pseudo-second-order equation is given as follows:

$$\frac{t}{q_t} = \frac{1}{k_2 q_e} + \frac{t}{q_e} \quad (16)$$

where k_2 is the second-order adsorption rate constant (g/mg/min). The constant k_2 is used to calculate the initial sorption rate 'h' (mg/(g min)), at $t \rightarrow 0$ by using

$$h = k_2 q_e \quad (17)$$

The straight line plots of t/q_t versus time (Fig. 5b) indicates that the adsorption data of Th(IV) ions fit well with pseudo-second-order kinetic model.

Elovich model

In reactions involving chemisorption of adsorbate on a solid surface without desorption of products, adsorption rate decreases with time due to an increased surface coverage. One of the most useful models for describing such 'activated' chemisorption is the Elovich equation (Rengaraj et al. 2007). Elovich equation is a rate equation based on the adsorption capacity describing the adsorption on highly heterogeneous adsorbent which is expressed as (Günay et al. 2007)

$$\frac{dq_t}{dt} = \alpha e^{-\beta q_t} \quad (18)$$

where α (mg/g/min) is the initial adsorption rate and β (g/mg) is the desorption constant related to the extent of surface coverage and activation energy for chemisorption (Fig. 5c).

The simplified equation is given as

$$q_t = \frac{\ln \alpha\beta}{\beta} + \frac{\ln t}{\beta} \quad (19)$$

assuming $\alpha\beta \gg t$ and $q_t = 0$ at $t = 0$ (Demirbaş and Alkan 2014).

Intra-particle diffusion

The solute transfer for a solid–liquid sorption process is usually characterized by external mass transfer (boundary layer diffusion) or intra-particle diffusion, or both. According to Kannan and Sundaram (Kannan and Sundaram 2001), an intra-particle diffusion coefficient K_{int} is given by the equation:

$$q_t = K_{int} t^{1/2} \quad (20)$$

where K_{int} is the intra-particle diffusion rate constant (mg/g/min$^{0.5}$). The plot of q_t versus $t^{0.5}$ (Fig. 5d) at different initial solution concentrations gives the value of K_{int}, and multilinearity indicates two or more steps occurring in the adsorption process which can be explained using the intra-particle diffusion model. The first sharper portion is the external surface adsorption or instantaneous adsorption stage which is relatively slow due to monolayer adsorption. The second portion is the gradual adsorption stage where the intra-particle diffusion rate is controlled. This involves capillary action where the metal ions adsorbed on the surface diffuse into the pores of the cellulose acetate beads and interact with the nano-Fe2O3 molecules, showing a rapid rate of adsorption. The third is the final equilibrium stage where intra-particle diffusion starts to slow down due to extremely low solute concentration in the solution and possible saturation of the adsorption sites.

The nonlinearized plots for the various models are presented in Fig. 5, and the various kinetic parameters are summarized in Table 3.

Thermodynamic studies

Thermodynamic parameters such as free energy change, enthalpy and entropy of the adsorption were determined based on Van't Hoff plot. The data were obtained under optimized conditions as mentioned earlier. The q_e value was observed to be in the range 21.3–18 mg/g for the temperature range 20–35 °C which decreases with increase in temperature ($\sim$11 mg/g at 50 °C), suggesting that the adsorption process is energy-dependent mechanism (Fig. 6a). The steep and sudden decrease in q_e at 50 °C indicates that the weak van der Waal's interaction, hydrogen bonding between thorium ions and active sites of beads brake at high temperature (Bayramoglu et al. 2006; Bhat et al. 2008).

The plot of $\ln K_d$ versus T^{-1} (Fig. 6b) yielded the thermodynamic parameters, such as enthalpy change (ΔH, in kJ/mol) and entropy (ΔS, in J/mol/K).

$$\ln K_d = (\Delta S/R) - (\Delta H/RT) \quad (21)$$

where K_d is the distribution coefficient

$$K_d = q_e/C_e \quad (22)$$

The change in Gibbs free energy was calculated from the equation

$$\Delta G = \Delta H - T\Delta S \quad (23)$$

where R is the universal gas constant = 8.314 J/mol/K and T is the absolute temperature (K).

The obtained values of ΔH and ΔS calculated from the plot of $\ln K_d$ versus $1/T$ are listed in Table 4.

The negative ΔH and ΔS values suggest exothermic process with high degree of randomness in adsorption of thorium ions, respectively. The positive values of ΔG indicate non-spontaneous adsorption of Th(IV) ions. Increase in temperature from 298 to 333 K results in increase in the positive ΔG value further confirming the non-spontaneous adsorption.

Table 3 Adsorption kinetic parameters

Conc. (mg/L)	Pseudo-second order			Pseudo-first order			Elovich model			Intra-particle diffusion
	k_2	q_e	R^2	k_1	q_e	R^2	α	β	R^2	K_{int}
25	0.0026	83.40	0.7395	0.0394	69.18	0.9098	0.649076	0.180	0.7999	1.94851
50	0.0081	32.16	0.7684	0.3832	34.67	0.8986	0.653829	0.179	0.9694	1.82997
75	0.0152	17.17	0.9094	0.0316	21.87	0.7608	0.582465	0.290	0.9176	1.13414
100	0.0189	8.30	0.9532	0.0311	9.31	0.9904	0.335384	0.555	0.9577	0.57928

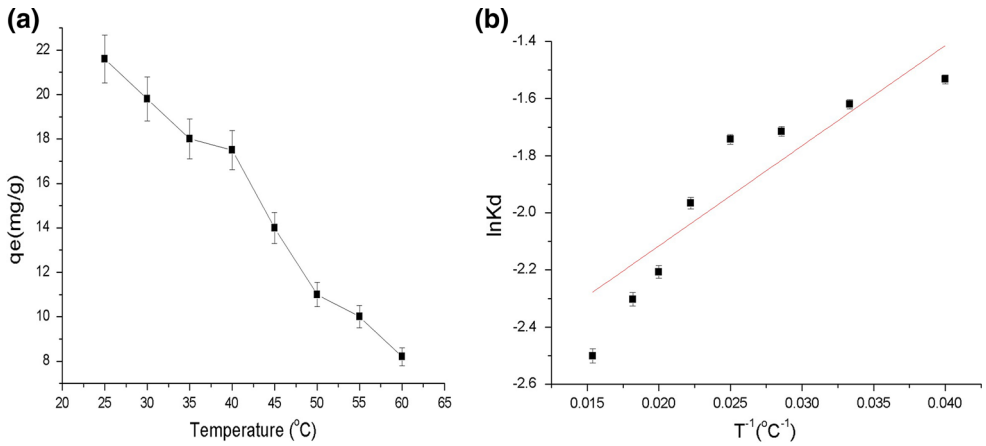

Fig. 6 Thermodynamics of adsorption. **a** Temperature dependence of adsorption capacity. **b** ln K_d versus T^{-1}

Table 4 Thermodynamic parameters

Co (mg/L)	pH	ΔH (kJ/mol)	ΔS (J/mol K)	ΔG (kJ/mol)				
				298 K	303 K	313 K	323 K	333 K
100	6	−0.291	−23.42	66.87	68.05	70.39	72.73	75.07

Recovery of Th(IV) ions

For economic viability and practical potential, the reusability of the fabricated beads was examined which was a major aim of the study. Instantaneous and effective diffusion of Th(IV) ions was observed from the hybrid cellulose matrix using 0.05N HNO3. The regenerative potential is clear, suggesting the reusability of the beads for industrial applications without any significant loss in the adsorption capacity for the Th(IV) ions which decreases with subsequent use. The recovery of beads can be attributed to the protonation at low pH and removal of the toxic metal ions simultaneously.

Conclusion

Nano-iron oxide (Fe_2O_3)-impregnated cellulose acetate composite was successfully synthesized as an effective adsorbent for the removal of Th(IV) ions from aqueous solution. The polymer exhibited distinct honeycomb-like surface morphology with the presence of well-defined flow lines and micropores. These adsorbent exhibited high affinity for the thorium(IV) ion with maximum adsorption capacity of 21.3 mg/g at 298 K. Adsorption was found to be highly pH dependent with maximum adsorption at pH of 6. The equilibrium adsorption correlated well with the Langmuir isotherm model with R^2 value of 0.9996 and followed the pseudo-first-order adsorption kinetics and the intra-particle diffusion model suggesting uniform monolayer formation. The reusability was remarkably noticed using 0.05N HNO_3 suggesting its potential use for industrial application.

Acknowledgments We would like to thank the Vice Chancellor Dr. Prahlada, DIAT (DU), for his support and help extended for this research activities; and Dr. O. Prakash (Ex-Head, Department of Ceramic Engineering, IIT (BHU), Varanasi), Dr. R. Pyare (Head, Department of Ceramic Engineering, IIT (BHU), Varanasi) and Dr.

P. Maiti (Coordinator, School of Materials Science & Technology, IIT (BHU), Varanasi) for the internship and thereby giving us an opportunity to work at DIAT. We would also thank Dr. Renuka R. Gonte, Nitish (VIT, Vellore), Fuhar Dixit and Tushar Sahetya (IIT-BHU) for their continued technical support.

References

Akkaya R, Akkaya B (2013) Adsorption isotherms, kinetics, thermodynamics and desorption studies for uranium and thorium ions from aqueous solution by novel microporous composite P (HEMA-EP). J Nucl Mater 434:328–333. doi:10.1016/j.jnucmat.2012.11.056

Aksu Z (2002) Determination of the equilibrium, kinetic and thermodynamic parameters of the batch biosorption of nickel(II) ions onto *Chlorella vulgaris*. Process Biochem 38:89–99. doi:10.1016/S0032-9592(02)00051-1

Anirudhan TS, Jalajamony S (2013) Ethyl thiosemicarbazide intercalated organophilic calcined hydrotalcite as a potential sorbent for the removal of uranium(VI) and thorium(IV) ions from aqueous solutions. J Environ Sci 25:717–725. doi:10.1016/S1001-0742(12)60064-3

Anirudhan TS, Rijith S, Tharun AR (2010) Adsorptive removal of thorium(IV) from aqueous solutions using poly (methacrylic acid)-grafted chitosan/bentonite composite matrix: process design and equilibrium studies. Colloids Surf A Physicochem Eng Asp 368:13–22. doi:10.1016/j.colsurfa.2010.07.005

Anirudhan TS, Radhakrishnan PG, Vijayan K (2013a) Development of a first-order kinetics based model, equilibrium studies, and thermodynamics for the adsorption of methyl orange onto a lignocellulosic anion exchanger. Sep Sci Technol 48:947–959. doi:10.1080/01496395.2012.715320

Anirudhan TS, Sreekumari SS, Jalajamony S (2013b) An investigation into the adsorption of thorium(IV) from aqueous solutions by a carboxylate-functionalised graft copolymer derived from titanium dioxide-densified cellulose. J Environ Radioact 116:141–147. doi:10.1016/j.jenvrad.2012.10.001

Ayalew A, Gonte RR, Balasubramanian K (2012) Development of polymer composite beads for dye adsorption. Int J Green Nanotechnol 4:440–454. doi:10.1080/19430892.2012.739480

Aydin FA, Soylak M (2010) Separation, preconcentration and inductively coupled plasma-mass spectrometric (ICP-MS) determination of thorium(IV), titanium(IV), iron(III), lead(II) and chromium(III) on 2-nitroso-1-naphthol impregnated MCI GEL CHP20P resin. J Hazard Mater 173:669–674. doi:10.1016/j.jhazmat.2009.08.137

Babel S, Kurniawan TA (2003) Low-cost adsorbents for heavy metals uptake from contaminated water: a review. J Hazard Mater 97:219–243

Baes CF, Meyer NJ, Roberts CE (1965) The Hydrolysis of thorium(IV) at 0 and 95°. Inorg Chem 4:518–527. doi:10.1021/ic50026a017

Baybaş D, Ulusoy U (2012) Polyacrylamide–hydroxyapatite composite: preparation, characterization and adsorptive features for uranium and thorium. J Solid State Chem 194:1–8. doi:10.1016/j.jssc.2012.07.039

Bayramoğlu G, Celik G, Arica MY (2006) Studies on accumulation of uranium by fungus Lentinus sajor-caju. J Hazard Mater 136:345–353. doi:10.1016/j.jhazmat.2005.12.027

Bhainsa KC, D'Souza SF (2009) Thorium biosorption by *Aspergillus fumigatus*, a filamentous fungal biomass. J Hazard Mater 165:670–676. doi:10.1016/j.jhazmat.2008.10.033

Bhat SV, Melo JS, Chaugule BB, D'Souza SF (2008) Biosorption characteristics of uranium(VI) from aqueous medium onto Catenella *repens*, a red alga. J Hazard Mater 158:628–635. doi:10.1016/j.jhazmat.2008.02.042

Borowiak-Resterna A, Cierpiszewski R, Prochaska K (2010) Kinetic and equilibrium studies of the removal of cadmium ions from acidic chloride solutions by hydrophobic pyridinecarboxamide extractants. J Hazard Mater 179:828–833. doi:10.1016/j.jhazmat.2010.03.078

Bulut E, Özacar M, Şengil İA (2008) Adsorption of malachite green onto bentonite: equilibrium and kinetic studies and process design. Microporous Mesoporous Mater 115:234–246. doi:10.1016/j.micromeso.2008.01.039

Cao C-Y, Cui Z-M, Chen C-Q et al (2010) Ceria hollow nanospheres produced by a template-free microwave-assisted hydrothermal method for heavy metal ion removal and catalysis. J Phys Chem C 114:9865–9870. doi:10.1021/jp101553x

Chen C, Wang X (2007) Sorption of Th(IV) to silica as a function of pH, humic/fulvic acid, ionic strength, electrolyte type. Appl Radiat Isot 65:155–163. doi:10.1016/j.apradiso.2006.07.003

Choy KKH, McKay G, Porter JF (1999) Sorption of acid dyes from effluents using activated carbon. Resour Conserv Recycl 27:57–71. doi:10.1016/S0921-3449(98)00085-8

Clark MW, Harrison JJ, Payne TE (2011) The pH-dependence and reversibility of uranium and thorium binding on a modified bauxite refinery residue using isotopic exchange techniques. J Colloid Interface Sci 356:699–705. doi:10.1016/j.jcis.2011.01.068

Demirbas O, Alkan M (2014) Adsorption kinetics of a cationic dye from wastewater. Desalin Water Treat 1–9. doi: 10.1080/19443994.2013.874705

DeZuane J (1997) Handbook of drinking water quality. Wiley, New York

El Samrani AG, Lartiges BS, Villiéras F (2008) Chemical coagulation of combined sewer overflow: heavy metal removal and treatment optimization. Water Res 42:951–960

Febrianto J, Kosasih AN, Sunarso J et al (2009) Equilibrium and kinetic studies in adsorption of heavy metals using biosorbent: a summary of recent studies. J Hazard Mater 162:616–645. doi:10.1016/j.jhazmat.2008.06.042

Frost A, Pearson R (1961) Kinetics and mechanism, second edition. J Phys Chem 65:384. doi:10.1021/j100820a601

Gonte R, Balasubramanian K (2013) Heavy and toxic metal uptake by mesoporous hypercrosslinked SMA beads: isotherms and kinetics. J Saudi Chem Soc

Gonte RR, Balasubramanian K, Mumbrekar JD (2013a) Porous and cross-linked cellulose beads for toxic metal ion removal: HG(II) ions. J Polym 2013:1–9. doi:10.1155/2013/309136

Gonte RR, Shelar G, Balasubramanian K (2013b) Polymer–agro-waste composites for removal of Congo red dye from wastewater: adsorption isotherms and kinetics. Desalin Water Treat 1–15. doi: 10.1080/19443994.2013.833876

Günay A, Arslankaya E, Tosun I (2007) Lead removal from aqueous solution by natural and pretreated clinoptilolite: adsorption equilibrium and kinetics. J Hazard Mater 146:362–371. doi:10.1016/j.jhazmat.2006.12.034

Hall KR, Eagleton LC, Acrivos A, Vermeulen T (1966) Pore- and solid-diffusion kinetics in fixed-bed adsorption under constant-pattern conditions. Ind Eng Chem Fundam 5:212–223. doi:10.1021/i160018a011

Hongxia Z, Zheng D, Zuyi T (2006) Sorption of thorium(IV) ions on gibbsite: effects of contact time, pH, ionic strength, concentration, phosphate and fulvic acid. Colloids Surf A Physicochem Eng Asp 278:46–52. doi:10.1016/j.colsurfa.2005.11.078

Hornback J (2005) Organic chemistry, 2nd edn, p 1328

Kannan N, Sundaram MM (2001) Kinetics and mechanism of removal of methylene blue by adsorption on various carbons—a comparative study. Dye Pigment 51:25–40

Kaygun AK, Akyil S (2007) Study of the behaviour of thorium adsorption on PAN/zeolite composite adsorbent. J Hazard Mater 147:357–362. doi:10.1016/j.jhazmat.2007.01.020

Kazy SK, D'Souza SF, Sar P (2009) Uranium and thorium sequestration by a *Pseudomonas* sp.: mechanism and chemical characterization. J Hazard Mater 163:65–72. doi:10.1016/j.jhazmat.2008.06.076

Klaine SJ, Alvarez PJJ, Batley GE et al (2008) Nanomaterials in the environment: behavior, fate, bioavailability and effects. Environ Toxicol Chem 27:1825. doi:10.1897/08-090.1

Kosarek L (1979) Radionuclide removal from water. Environ Sci Technol 13:522–525. doi:10.1021/es60153a609

Kütahyalı C, Eral M (2010) Sorption studies of uranium and thorium on activated carbon prepared from olive stones: kinetic and thermodynamic aspects. J Nucl Mater 396:251–256. doi:10.1016/j.jnucmat.2009.11.018

Langmuir D, Herman JS (1980) The mobility of thorium in natural waters at low temperatures. Geochim Cosmochim Acta 44:1753–1766

Marmolejo-Rodríguez AJ, Caetano M, Prego R, Vale C (2008) Thorium accumulation in the sedimentary environment of the Vigo Ria (NW Iberian Peninsula). J Environ Radioact 99:1631–1635. doi:10.1016/j.jenvrad.2008.06.008

Metaxas M, Kasselouri-Rigopoulou V, Galiatsatou P et al (2003) Thorium removal by different adsorbents. J Hazard Mater 97:71–82

Nilchi A, Shariati Dehaghan T, Rasouli Garmarodi S (2013) Kinetics, isotherm and thermodynamics for uranium and thorium ions adsorption from aqueous solutions by crystalline tin oxide nanoparticles. Desalination 321:67–71. doi:10.1016/j.desal.2012.06.022

Pereira FJ, Díez MT, Aller AJ (2013) Synthesis and characterization of arsenic-doped cysteine-capped thoria-based nanoparticles. J Nanoparticle Res 15:1895. doi:10.1007/s11051-013-1895-8

Prabhakar S, Misra BM, Roy SB et al (1994) Reverse osmosis separation of radiocontaminants from ammonium diuranate effluents. Sep Sci Technol 29:1001–1010. doi:10.1080/01496399408005613

Raje N, Reddy AVR (2010) Mechanistic aspects of thermal decomposition of thorium oxalate hexahydrate: a review. Thermochim Acta 505:53–58. doi:10.1016/j.tca.2010.03.025

Rengaraj S, Kim Y, Joo CK et al (2004) Batch adsorptive removal of copper ions in aqueous solutions by ion exchange resins: 1200H and IRN97H. Korean J Chem Eng 21:187–194. doi:10.1007/BF02705397

Rengaraj S, Yeon J-W, Kim Y et al (2007) Adsorption characteristics of Cu(II) onto ion exchange resins 252H and 1500H: kinetics, isotherms and error analysis. J Hazard Mater 143:469–477. doi:10.1016/j.jhazmat.2006.09.064

Rule P, Balasubramanian K, Gonte RR (2014) Uranium(VI) remediation from aqueous environment using impregnated cellulose beads. J Environ Radioact 136:22–29. doi:10.1016/j.jenvrad.2014.05.004

Sarkar M, Acharya PK, Bhattacharya B (2003) Modeling the adsorption kinetics of some priority organic pollutants in water from diffusion and activation energy parameters. J Colloid Interface Sci 266:28–32

Seyhan S, Merdivan M, Demirel N (2008) Use of o-phenylene dioxydiacetic acid impregnated in Amberlite XAD resin for separation and preconcentration of uranium(VI) and thorium(IV). J Hazard Mater 152:79–84. doi:10.1016/j.jhazmat.2007.06.065

Shoushtari AM, Zargaran M, Abdouss M (2006) Preparation and characterization of high efficiency ion-exchange crosslinked acrylic fibers. J Appl Polym Sci 101:2202–2209. doi:10.1002/app.23465

Shtangeeva I, Ayrault S, Jain J (2005) Thorium uptake by wheat at different stages of plant growth. J Environ Radioact 81:283–293. doi:10.1016/j.jenvrad.2004.01.041

Soylak M, Erdogan ND (2006) Copper(II)-rubeanic acid coprecipitation system for separation-preconcentration of trace metal ions in environmental samples for their flame atomic absorption spectrometric determinations. J Hazard Mater 137:1035–1041. doi:10.1016/j.jhazmat.2006.03.031

Sunta CM, Dang HS, Jaiswal DD (1987) Thorium in man and environment uptake and clearance. J Radioanal Nucl Chem 115:149–158

Talip Z, Eral M, Hićsönmez U (2009) Adsorption of thorium from aqueous solutions by perlite. J Environ Radioact 100:139–143. doi:10.1016/j.jenvrad.2008.09.004

Uluozlu OD, Tuzen M, Mendil D, Soylak M (2010) Coprecipitation of trace elements with Ni2 +/2-Nitroso-1-naphthol-4-sulfonic acid and their determination by flame atomic absorption spectrometry. J Hazard Mater 176:1032–1037. doi:10.1016/j.jhazmat.2009.11.144

Ünak T (2000) What is the potential use of thorium in the future energy production technology? Prog Nucl Energy 37:137–144. doi:10.1016/S0149-1970(00)00038-X

Valković V (2000) Radioactive nuclides in nature. In: Radioactivity in the environment, 1st edn. Elsevier, pp 5–32

Yuan G (2004) Natural and modified nanomaterials as sorbents of environmental contaminants. J Environ Sci Heal A 39:2661–2670. doi:10.1081/ESE-200027022

Zhang L, Fang M (2010) Nanomaterials in pollution trace detection and environmental improvement. Nano Today 5:128–142

Zhang S, Liu P, Zhang B (2005) Thorium resources and their availability. World Nucl Geosci 2:9

Zhao DL, Feng SJ, Chen CL et al (2008) Adsorption of thorium(IV) on MX-80 bentonite: effect of pH, ionic strength and temperature. Appl Clay Sci 41:17–23

Zhao Y, Li J, Zhang S et al (2013) Efficient enrichment of uranium(VI) on amidoximated magnetite/graphene oxide composites. RSC Adv 3:18952. doi:10.1039/c3ra42236d